Inorg. Chem. **2006**, *45*, 2704–2712

Inorganic Chemistry
Article

Synthesis of Thin Cr_3Se_4 Films from Modulated Elemental Reactants via Two Amorphous Intermediates: A Detailed Examination of the Reaction Mechanism

Malte Behrens, Ragnar Kiebach, and Wolfgang Bensch*

Institut für Anorganische Chemie, Christian-Albrechts-Universität zu Kiel, Olshausenstrasse 40–60, D-24098 Kiel, Germany

Dietrich Häussler and Wolfgang Jäger

Mikrostrukturanalytik, Technische Fakultät, Christian-Albrechts-Universität zu Kiel, Kaiserstrasse 2, D-24143 Kiel, Germany

Received September 6, 2005

The reaction of Cr/Se multilayers when they are annealed occurs in two steps: interdiffusion of the single layers to an amorphous Cr–Se alloy and crystallization of Cr_3Se_4. Both reaction steps were characterized using various techniques. At approximately 300 °C the layers have interdiffused completely to form a homogeneous amorphous Cr–Se alloy. Short-range order in the alloy was probed with X-ray absorption spectroscopy (XAS) and, according to the results of this, is already very similar to Cr_3Se_4, which crystallizes around 500 °C. Crystallization occurs at a well-defined temperature, whereas crystallite growth proceeds in the whole temperature interval above the crystallization temperature and is not finished at 660 °C. The reaction yields a polycrystalline thin film of Cr_3Se_4 in a preferred orientation exhibiting a (00*l*) texture. In Cr-rich samples amorphous Cr is present as a by-product. A Cr–Se/Se multilayer was observed as an intermediate in the interdiffusion of some Cr-rich samples which is stable between 200 and 250 °C.

Introduction

Enormous efforts were undertaken in the past decades in the field of thin films and coatings by solid-state chemists, material scientists, and physicists. The unique properties of thin films may be exploited to control the surface properties of materials for various applications. Many functional layers do not exhibit the required properties in the as-deposited state, but receive their special properties after a solid-state chemical reaction of the reactants; i.e., a subsequent annealing procedure introduces the required properties of the material. The thin film approach may thus be regarded as an important synthetic method for solid-state chemists. Understanding reactions of film couples might be a key for researchers to influence the properties of the final thin film.

From an academic perspective, thin film technology also grants unique insights into the solid state. Reaction interfaces in multilayer thin films can be tailored a priori by variation of the single layer deposition sequence. Interfaces are much more easily characterized with special techniques than reaction interfaces in classical high-temperature reactions using polycrystalline starting materials. A close look onto the fundamental steps of solid-state reactions such as diffusion, nucleation, and crystal growth may be obtained using thin multilayer films as reactants.[1] This makes the so-called modulated elemental reactant method a powerful tool for the understanding of reaction mechanisms in solid-state chemical reactions. The thin film approach is characterized by short diffusion paths, low reaction temperatures, partial control of the intermediates, and the possibility of obtaining kinetically stable products. Pioneering work in this field was done by Johnson and his group.[1−3]

In typical multilayer film reactions the elemental reactants are deposited in an alternating fashion on an appropriate

* Corresponding author. E-mail: wbensch@ac.uni-kiel.de. Fax: +49 (0)431/880-1520.

(1) Fister, L.; Novet, T.; Grant, C. A.; Johnson, D. C. In *Advances in the Synthesis and Reactivity of Solids*, Vol. 2; Mallouk, T. E., Ed.; JAI Press: London, 1994; pp 155−234.
(2) Noh, M.; Johnson, C. D.; Hornborstel, M. D.; Thiel, J.; Johnson, D. C. *Chem. Mater.* **1996**, *8*, 1625−1635.
(3) Johnson, D. C. *Curr. Opin. Solid State Mater. Sci.* **1988**, *3*, 159−167.

10.1021/ic0515204 CCC: $33.50 © 2006 American Chemical Society
Published on Web 02/16/2006

substrate. The reactant systems are usually X-ray amorphous in the high scattering angle region, and a distinct heat treatment yields crystalline products. Two different reaction pathways depending on the thickness of the repeating layer are established for some systems: Thick films tend to nucleate crystalline products at the single layer interfaces, while in thinner films first a complete interdiffusion of the constituents is observed. In the latter samples an amorphous alloy is formed, and at a distinct temperature nucleation and growth of crystalline products occur in a second step. A "critical thickness" exists in such systems directing the reaction in either way.[4]

Binary systems of transition metal chalcogenides attracted a lot of attention with the modulated elemental reactant method.[5−12] Encouraged by the successful work of Johnson and his group in several transition metal selenide systems[5−8,13−16] and our recent results obtained in the Cr−Te system,[10−12] we chose the multilayer method to synthesize chromium selenides and explored their building mechanism. Chromium selenides exhibit interesting structural, magnetic, and electrical properties. Some chromium chalcogenides are promising candidates for half-metallic ferromagnets that are seen as key ingredients for spintronic applications.[17] For this purpose, thin film technology is required. A brief summary of known binary Cr−Se phases containing the most important references was given by Huppertz et al.[18] The syntheses in the present study always yield Cr_3Se_4. As the neighboring phases Cr_2Se_3 and Cr_7Se_8, Cr_3Se_4 crystallizes in the monoclinic crystal system in space group *I*2/*m*.[19] The structure can be derived from the NiAs structure type by introducing vacancies in every second metal atom layer. The concentration of vacancies is variable to a certain extent, and the compositional range was determined to $Cr_{3\pm x}Se_4$ with $0 < x < 0.2$.[20] A reversible order−disorder transition was observed for Cr_3Se_4 at 900 °C, yielding a defect-CdI_2 structure.[21] Monoclinic Cr_3Se_4 exhibits a small electronic band gap[22] and shows a conductivity typical for poor metals.[20] The compound aroused some interest because of its complicated magnetic properties that strongly depend on the exact composition $Cr_{3\pm x}Se_4$.[20−25] For Cr-rich materials ($x > 0$) antiferromagnetic behavior occurs, and for Cr-poor samples ($x < 0$) meta- or ferromagnetic order was observed. At temperatures above 90 K a Curie−Weiss law is obeyed with $\theta < 0$ K for $x > 0$ and $\theta > 0$ K for $x < 0$. For Cr-rich samples a static Jahn−Teller distortion due to the introduction of further Cr^{2+} (d^4) is observed. Bulk Cr_3Se_4 is usually prepared from the elements by a high-temperature procedure.

Experimental Section

Multilayer films were prepared in an ultrahigh-vacuum deposition chamber ($p < 10^{-8}$ mbar), which is described in detail elsewhere.[26] Cr and Se were deposited on (100) silicon single-crystal substrates to form 10 or 50 Cr/Se double layers. The substrate size for all samples was approximately 1 cm^2. Including the substrate, samples can be described as [Si/native SiO_x/$(Cr/Se)_n$] ($n = 10$ or 50). Chromium powder (Chempur, 99.99%) was deposited with a Focus EFM 3 electron beam gun with a flux of 1 μA. The flux was held at a constant level and controlled by a flux monitor. A Knudsen cell controlled by an Oxford Instruments temperature controller was used to evaporate Selenium at 240 °C (Se: Riedel-de Haen, 99.9%). Single-layer thicknesses were controlled by adjusting the shutter opening time interval of the evaporation cells. The evaporation rates were previously determined using quartz crystal thickness monitors (Tectra) and calibration samples. The evaporation rate amounts to 0.3 Å/min for Cr, whereas the Se deposition rate was found to vary slightly as a function of the level of crucible filling, and typical values are between 0.1 and 0.2 Å/min. This is the reason that some samples showed a slight deviation from the intended values. Compositions were controlled using previous multilayer samples as references. The substrate was kept at ambient temperatures in all experiments. Bulk Cr_3Se_4 was used as a reference sample in X-ray absorption spectroscopy and was prepared from the elements at 900 °C in evaporated silica ampules.

X-ray data were collected on a Bruker-AXS D8 Advance $\theta-\theta$ diffractometer (Cu Kα radiation) equipped with a Göbel mirror and a Material Research Instruments Reflectometry high-temperature chamber (MRI−HTC). In situ experiments were performed under high vacuum ($p < 10^{-5}$ mbar). The temperature was gradually increased in steps of 10 or 20 °C with a heating rate of 0.05 or 0.1 °C/s and held constant during the collection of XRD patterns. The crystallite size was determined by applying a line profile analysis (LPA).[27] As a standard, high-quality SiO_2 was used to account for instrumental line broadening. XRR (X-ray reflectometry) experiments and ex situ XRD were performed on a reflectometry sample stage in air on the same machine.

(4) Gösele, U.; Tu, K. N. *J. Appl. Phys.* **1989**, *66*, 2619−2626.
(5) Fukuto, M.; Hornborstel, M. D.; Johnson, D. C. *J. Am. Chem. Soc.* **1994**, *116*, 9136−9140.
(6) Oyelaran, O.; Novet, T.; Johnson, C. D.; Johnson, D. C. *J. Am. Chem. Soc.* **1996**, *118*, 2422−2426.
(7) Moss, S.; Noh, M.; Jeong, K. H.; Kim, D. H.; Johnson, D. C. *Chem. Mater.* **1996**, *8*, 1853−1857.
(8) Overbay, M.; Novet, T.; Johnson, D. C. *J. Solid State Chem.* **1996**, *123*, 337−343.
(9) Schneidmüller, R.; Hornborstel, M. D.; Johnson, D. C. *Inorg. Chem.* **1997**, *36*, 5894−5899.
(10) Kraschinski, S.; Herzog, S.; Bensch, W. *Solid State Sci.* **2002**, *4*, 1237−1243.
(11) Herzog, S.; Kraschinski, S.; Bensch, W. *Z. Anorg. Allg. Chem.* **2003**, *629*, 1825−1832.
(12) Riemenschneider, O. Ph.D. Thesis, University of Kiel, Germany, 2003.
(13) Noh, M.; Johnson, D. C. *Chem Mater* **2000**, *12*, 2894−2901.
(14) Hughes, T. A.; Kevan, S. D.; Cox, D. E.; Johnson, D. C. *J. Am. Chem. Soc.* **2000**, *122*, 8910−8915.
(15) Noh, M.; Thiel, J.; Johnson, D. C. *Adv. Mater.* **1996**, *8*, 596−599.
(16) Noh, M.; Johnson, D. C. *Angew. Chem., Int. Ed. Engl.* **1996**, *35*, 2666−2669.
(17) Xie, W. H.; Xu, Y. Q.; Liu, B. G.; Pettifor, D. G. *Phys. Rev. Lett.* **2003**, *91*, 037204−01.
(18) Huppertz, H.; Lühmann, H.; Bensch, W. *Z. Naturforsch.* **2003**, *58b*, 934−938.
(19) Chevreton, M.; Murat, M.; Eyraud, C. *J. Phys. (Paris)* **1963**, *24*, 443−446.
(20) Maurer, A.; Collin, G. *J. Solid State Chem.* **1980**, *34*, 23−30.
(21) Ohtani, T.; Fujimoto, R.; Yoshinaga, H.; Nakahira, M.; Ueda, Y. *J. Solid State Chem.* **1983**, *48*, 161−167.
(22) Ivanova, V. A.; D. Sh. Abdinov, Aliev, G. M. *Phys. Status Solidi* **1967**, *24*, K145−K147.
(23) Babot, D.; Chevreton, M.; Buevoz, J. L.; Langnier, R.; Lambert-Andron, B.; Winterberger, M. *Solid State Commun.* **1979**, *30*, 253−257.
(24) Winterberger, M.; André, G.; Hammann, J. *J Magn. Magn. Mater.* **1995**, *147*, 167−176.
(25) Dijkstra, J.; van Bruggen, C. F.; Haas, C.; deGroot, R. A. *J. Phys. Condens. Matter* **1989**, *1*, 9163−9174.
(26) Lokuschus, K.; Kraschinski, S.; Herzog, S.; Bensch, W. *Rev. Sci. Instrum.* **2001**, *72*, 4297−4299.
(27) Langford, J. I. In *Industrial Applications of X-ray Diffraction*; Chung, F. H., Smith, D. K., Eds.; Marcel Dekker Inc.: New York, 2000; pp 847−867.

Se K-edge spectra of Cr−Se films and reference samples were collected at room temperature at the X1 beamline of HASYLAB at DESY, Hamburg, Germany, using the Si(111) monochromator. Fluorescence spectra of the thin films were taken by placing the sample in a 45° angle with respect to the beam and placing a Ge fluorescence detector perpendicular to it. Reference spectra of Se and Cr_3Se_4 were measured in transmission geometry and with application of ionization chambers. Near-edge structure (XANES) and extended fine structure (EXAFS) spectra were analyzed with the software WinXAS[28] and FEFF8.[29] Evaluation of Fourier transformed EXAFS (FT-EXAFS) spectra were performed using models for coordination clusters around the absorbing Se atom. Theoretical spectra were calculated ab initio using the FEFF code and fitted to the experimental data. The number of refined parameters was kept as low as possible. Reasonable fits were obtained using one expansion parameter per cluster for the interatomic distances, one Debye−Waller factor per element, and one E_0 shift parameter per element. The E_0 shifts of the Se and Cr sublattices were refined for the as-deposited sample (CS09) and the crystalline Cr_3Se_4 film (CS08), respectively, and kept constant for the other thin film samples. The S_0^2 parameter was fixed to 0.9 for all samples. Coordination numbers (CN) were set to 2 for the Se−Se contacts in the samples CS09 and CS18 and to 4.5 in the sample CS13, according to the single-crystal structure of Cr_3Se_4 for the first shell.

The compositions of the films were determined in a Philips scanning electron microscope (SEM) XL 30 ESEM equipped with an EDAX system. Due to the very small amount of material and the strong substrate peak an accuracy of about 5 at. % was reached. Atomic force microscopy (AFM) pictures of the samples were obtained with a Park Autoprobe CP scanning probe microscope with a 5 μm scanner in contact AFM mode. TEM micrographs and electron diffraction patterns were recorded on a Philips CM30 STEM at 300 kV. For this purpose a free-standing film was prepared by removing the Si wafer from the backside of the sample by subsequent grinding, dimpling, and ion bombardment.

Results and Discussion

In Table 1 are compiled the samples made as part of this investigation. The aim was to synthesize samples of varying composition across the Cr−Se phase diagram. The samples cover Cr contents between 14(5) and 67(5) at. % and Cr/Se double layer thicknesses between 30(2) and 200(3) Å (Table 1). The chemical reaction of the multilayer samples upon annealing was investigated with in situ XRR and XRD. Three different parts of the reaction can clearly be distinguished, and an overview is given in Figure 1. First, from room temperature to approximately 300 °C, the components of the single layers interdiffuse, which is indicated by the decay of the superstructure reflections. Afterward (300−500 °C), an amorphous alloy occurs as a reaction intermediate. Finally, nucleation and growth of crystalline Cr_3Se_4 is detected. The XANES, EXAFS, and Fourier transformed EXAFS (FT-EXAFS) spectra of selected samples obtained after different annealing temperatures and reference spectra of Se and bulk Cr_3Se_4 were recorded to probe the development of short-range order around the Se atoms (Figure 2). Results of the fitting procedures of EXAFS spectra for all samples are summarized in Table 2. All parts of the reaction will be discussed in detail in the following sections.

Table 1. Characteristic Data of the 19 Cr/Se Multilayer Films Investigated[a]

sample	Cr/Se double layers	double layer thickness/Å	Cr content/ (at. %)	Intended thickness inÅ/Cr content as at. %/
CS03	10	73(1)	65(5)	70/66
CS04	10	19(2)[b]	45(5)	20/50
CS05	10	35(1)	49(5)	35/50
CS06	10	54(4)	23(5)	55/25
CS07	10	42(1)	50(5)	40/50
CS08	10	200(3)	19(5)	200/20
CS09	50	58(2)	14(5)	60/20
CS10	10	54(1)	60(5)	60/60
CS11	10	47(1)	59(5)	50/50
CS12	50	30(2)	50(5)	30/50
CS13	10	53(2)	46(5)	55/43
CS15	10	135(4)	32(5)	125/30
CS16	10	79(3)	35(5)	80/35
CS17	50	77(2)	41(5)	80/43
CS18	10	60(1)	67(5)	60/70
CS21	50	37(3)	36(5)	40/40
CS22	10	145(2)	22(5)	150/20
CS23	50	60(3)	36(5)	60/40
CS24	50	55(4)	27(5)	60/30

[a] Errors of the double layer thicknesses were estimated on the basis of the quality of the XRR data (intensity and number and width of multilayer Bragg peak). [b] No multilayer Bragg peak was visible for this sample, indicating that the reactants have completely interdiffused at room temperature. The thickness of the "repeating unit" was determined from Kiessig fringes.

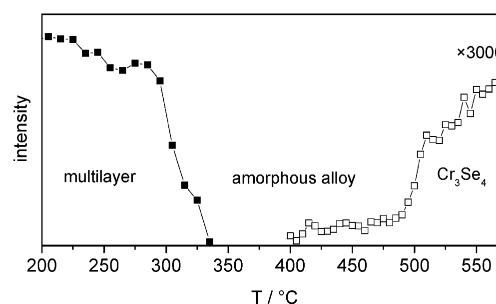

Figure 1. Reaction of sample CS03 upon annealing. At low temperatures the interdiffusion of the single Cr and Se layers is probed by the decay of the first-order superstructure satellite (closed symbols). Starting at about 300 °C a nonmodulated X-ray amorphous Cr/Se alloy exists, and at about 500 °C Cr_3Se_4 crystallizes. The open symbols denote the intensity of the (002) reflection of Cr_3Se_4.

The first characterization of the as deposited multilayers was done using XRR to probe the layered nature of the samples. The quality of XRR patterns was found to improve with increasing Cr content of the samples. This might be due to the fact that the Se layers exhibit a much larger roughness than the Cr layers, i.e., a high Se content decreases the quality of the layer system. Nevertheless, Bragg peaks caused by the modulation are visible in the XRR measurements of most samples. In Cr rich samples additional Kiessig fringes and higher order multilayer peaks are detected (Figure 3). The modulation wavelength of the multilayer, which is the thickness of the repeating double layer for binary systems, can be determined from the XRR curves using a Bragg law that is modified by the influence of refraction:[30]

$$D = \frac{m\lambda}{2\sqrt{\sin^2\theta_m - \sin^2\theta_C}} \qquad (1)$$

(28) Ressler, T. WinXAS V3.1, 1994−2004.
(29) Ankudinov, A. L.; Ravel, B.; Rehr, J. J.; Conradson, S. D. *Phys. Rev. B* **1998**, 7565.

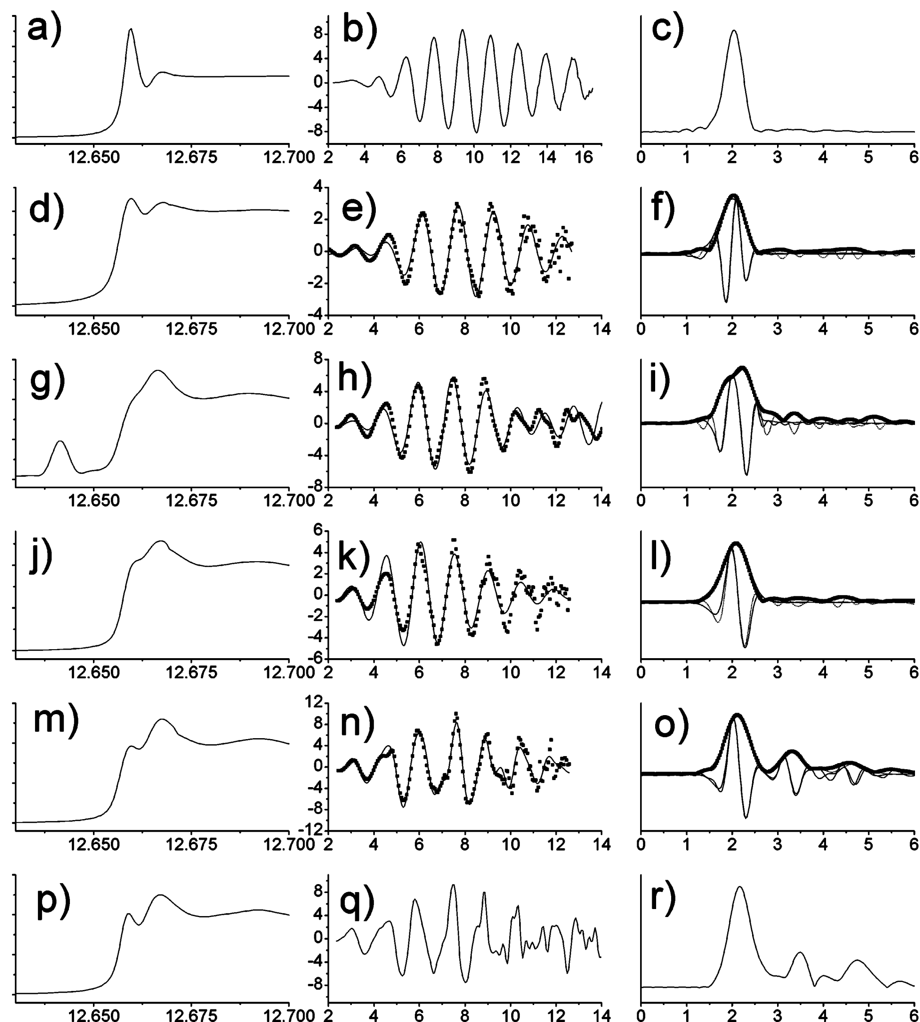

Figure 2. XAS spectra for four Cr/Se thin film samples and references: XANES, $\chi(k)$ (k^3-weighted) and FT-EXAFS spectra (magnitude and imaginary part) for the Se reference (a−c), sample CS09 (as deposited, d−f), sample CS18 (interdiffusion intermediate, heated to 180 °C, g−i), sample CS13 (amorphous alloy, heated to 300 °C, j−l), sample CS08 (crystalline, heated to 660 °C, m−o), and the Cr_3Se_4 bulk reference (p−r). The symbols denote experimental data, and the solid lines, the fits of theoretical spectra in f, i, l, and o.

Table 2. Structural Data for the First Coordination Shell of the Se Atoms in Cr/Se Thin Film Samples after Annealing at Different Temperatures[a]

sample	annealing temp/°C	bonds to	CN	bonding distance/Å	DW factor	E_0 shift	remark
CS09	RT	Se	2^b	2.36(1)	0.00938(1)	6.6(1)	as deposited
CS18	180	Se	2^b	2.33(1)	0.00405(1)	6.6^b	interdiffusion intermediate
		Cr	4^b	2.55(1)	0.00278(1)	8.0^b	
CS13	300	Cr	4.5^b	2.51(1)	0.0125(1)	8.0^b	amorphous alloy
CS08	650	Cr	4.5^b	2.51(1)	0.00748(1)	8.0(1)	crystalline Cr_3Se_4

[a] Results are obtained from Se−K EXAFS fits. For the sample CS08 the crystal structure of Cr_3Se_4 was chosen as the cluster model and the values given here are averaged over nine different Se−Cr bonds. [b] Parameter fixed during refinement.

where D is the double-layer thickness, m is the order of the multilayer reflection, θ_m is the angular position of the multilayer reflection, and θ_c is the critical angle for the multilayer. The critical angle is located where the reflected intensity is 50% of the total external reflection.[31] Additional to θ_c of the multilayer, θ_c of the Si substrate can also be observed at an incident angle of 0.22°. At such low angles, the illuminated area is larger than the size of the deposited multilayer system and reflection from the uncovered substrate is observed. Superstructure reflections are detected up to the fifth order for sample CS18, as shown in Figure 3. Kiessig fringes are due to interference of the waves that were reflected at the air/multilayer and the multilayer/substrate interfaces and correspond to the total film thickness. The repeating double layer thicknesses of each sample are summarized in Table 1. Except for the superstructure reflections and those of the silicon substrate no other Bragg peaks are seen in the XRD patterns of the as-deposited films, indicating that the materials were X-ray amorphous. FT-EXAFS spectra show that in the as-deposited film Se is surrounded by a single ordered coordination shell (Figure 2f). With only Se−Se contacts in the separated single layers, the interatomic distance amounts to 2.36(1) Å. This is slightly

(30) Holý, V.; Pietsch, U.; Baumbach, T. *High-Resolution X-ray Scattering form Thin Films and Multilayers*; Springer-Verlag: Berlin, 1999; pp 119−149.
(31) Parrat, L. G. *Phys. Rev.* **1954**, *95*, 359−369.

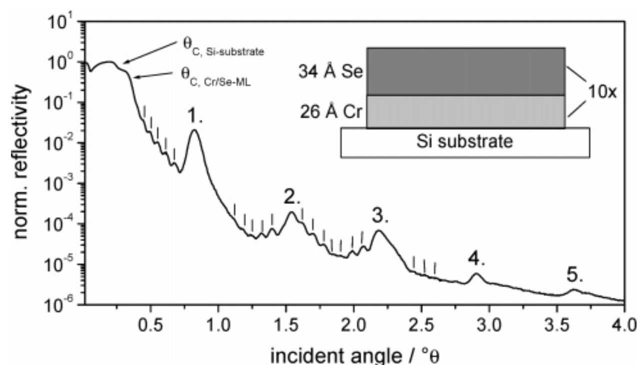

Figure 3. XRR pattern of the sample CS18 as deposited. The critical angles of the Si substrate and the multilayer are marked. The numbers denote the diffraction order of the multilayer satellite peaks. Kiessig fringes are denoted with a vertical line. The model of the multilayer sample calculated from XRR data and the composition (assuming bulk densities) is shown in the upper right corner.

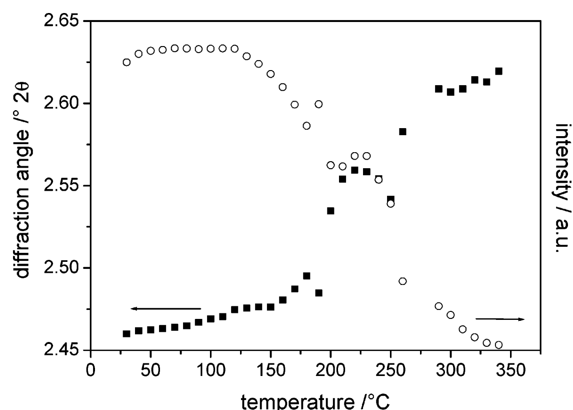

Figure 4. Intensity (open symbols) and position (closed symbols) of the first-order superstructure satellite peak of the sample CS05 upon annealing.

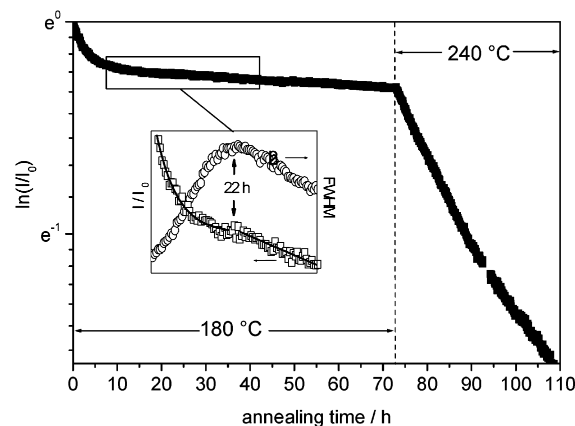

Figure 5. Normalized intensity of the first-order direct beam superstructure satellite peak of the sample CS18 upon isothermal annealing at 180 and 240 °C. After about 22 h at 180 °C a change of the interdiffusion rate is detected. This is attributed to the formation of an intermediate (inset, squares; lines drawn visually). The half-width of the peaks decreases after this first interdiffusion step (inset, circles).

larger than in the Se reference and earlier studies on amorphous bulk Se, where 2.33 Å was found.[32] CN was fixed to 2, which is the typical CN in amorphous Se.[32] These results are assumed to be representative for the Se single layers in all samples.

In situ XRR revealed that the first step of the reaction is due to interdiffusion of the single layers. Superstructure satellites in XRR patterns of multilayers are an excellent probe to investigate this process.[33] Intensity and position of the first-order superstructure reflection of sample CS05 are plotted vs T in Figure 4. Two effects are obvious: The intensity decreases, indicating the gradual destruction of the multilayer modulation; the position of the reflection shifts toward higher angles, indicating a simultaneous shrinking of the repeating double-layer thickness. The latter effect is caused by the densification of the sample. Thin films prepared by vapor deposition techniques usually have a lower density than bulk samples for example due to columnar growth and different defects.[34] Increasing density upon annealing is often observed in such films. It amounts to about 7% for the present sample. A chemical factor also contributes to the densification. The sum of a Se−Se and a Cr−Cr bond length is about 8% longer than two Cr−Se bonds, using bcc-Cr, α-Se and Cr_3Se_4 as references. The strong compaction indicates that pronounced structural relaxation proceeds in the amorphous multilayers when they are annealed.

It can be seen from Figure 4 that the reflection position and intensity of the sample CS05 both remain almost constant in the temperature range of 200−250 °C. Hence, it can be assumed to be the range of existence of an interdiffusion intermediate. An isothermal annealing experiment was performed on the sample CS18 at 180 °C. The decay of the first-order superstructure reflection as a function of time is shown in Figure 5. The interdiffusion is fast and nonlinear at the beginning and slows down rapidly with increasing reaction time. After about 15 h the decay is linear. In amorphous multilayers the slow down of interdiffusion can be attributed to stress effects.[35] Fast and nonlinear interdiffusion at the beginning occurs prior to the development of stress in the film, and the structural relaxation governs the rate of interdiffusion. In the linear part of the curve the rate-limiting step is stress relief, which may occur by viscous flow of the material. Similar behavior was also reported and explained qualitatively and quantitatively for other amorphous multilayer systems.[36−38]

An additional abrupt slow down of the interdiffusivity is detected after about 22 h (Figure 5, inset). We attribute this change of the interdiffusion rate to the formation of the intermediate. Gösele and Tu predicted an intermediate modulated structure for samples with significantly different single-layer thicknesses.[4] In such a case the thinner layer is consumed completely before the thicker one when the binary phase is formed at the interface. Afterward, the binary phase is sandwiched by the residual thicker supply layers. In sample CS18 the individual layer thickness can be calculated from

(32) Federcio, M.; Galli, G.; Majolino, D. *Nuovo Cimento Soc. Ital. Fis.* **1998**, *10D*, 425−434.
(33) Greer, A. L. *Curr. Opin. Solid State Mater. Sci.* **1997**, *2*, 300−304.
(34) Ohring, M. in *The Material Science of Thin Films*; Academic Press: London, 1992; pp 195−248.
(35) Greer, A. L. *Diffus. Defect Data, Pt. A* **1996**, *129−130*, 163−180.
(36) Stephenson, G. B. *Diffus. Defect Data, Pt. A* **1993**, *95−98*, 507−518.
(37) Greer, A. L. *Annu. Rev. Mater. Sci.* **1987**, *17*, 219−233.
(38) Mizoguchi, T.; Murata, M. *Jpn. J. Appl. Phys.* **1991**, *30*, 1818−1821.

the composition and the modulation wavelength assuming bulk densities. The values are about 26 Å for the Cr layers and 34 Å for Se. The error introduced using bulk densities can be justified, because such densities are taken for both single layers and therefore will outbalance itself to a certain extent. The difference between the thickness of the individual layers leads to a complete consumption of the thinner Cr layer in the first step of the interdiffusion process as the Cr/Se phase is formed at the interfaces. The intermediate structure of the sample CS18 can then be described as a $[(Cr-Se)/Se]_{10}$ multilayer. Simultaneously to the change of the interdiffusion rate, a decrease of the half-width of the superstructure reflection is detected (Figure 5, inset). This can be interpreted as the homogenization of the repeating layer thickness of the $[(Cr-Se)/Se]_{10}$ multilayer system, compared to the as-deposited $[Cr/Se]_{10}$ structure.

The interdiffusion of CS18 was interrupted at the stage of the intermediate material. The sample was investigated with XAS at the Se−K edge. It can be seen from the XANES that the local environment of the Se atoms changes dramatically during the interdiffusion process (Figure 2d,g,j). The XANES of the interdiffusion intermediate exhibits a preedge peak (Figure 2g), which is a typical feature of the $1s-t_2^*$ transition for a tetrahedral coordination environment. It can thus be assumed that after the first interdiffusion step the intermediate contains Se residing in a tetrahedral coordination of four Cr atoms in the Cr−Se layers. A tetrahedral coordination of Se by Cr is very unusual in chromium selenides, where normally a hexagonal packing of Se anions with Cr residing in the octahedral voids is observed. According to the overall composition of the sample, the binary interdiffused phase must be relatively Cr rich, because some Se still resides in the supply layers. It can be assumed that the hexagonal packing of Se is inhibited by the vast excess of Cr, which leads to the unusual tetrahedral coordination.

In the interdiffusion intermediate of CS18 an additional peak in the FT-EXAFS spectra indicates a new coordination shell (Figure 2i). The Se−Se peak is still present and can be seen as a shoulder on the lower distance side of the new peak. Comparing the present spectrum with that of the completely interdiffused sample with only Se−Cr contacts (Figure 2l), the new shell should contain Cr. The Se−Cr distance is 2.55(1) Å, and Se−Se contacts are shortened to 2.33(1) Å due to the compaction of the material. It is most likely that these Se−Se contacts are located in the remaining Se supply layer, whereas the $SeCr_4$ clusters are formed in the newly developing Cr−Se layers. The coexistence of Se−Se and Se−Cr coordination in the sample confirms the $[(Cr-Se)/Se]_{10}$ multilayer structure of the interdiffusion intermediate of CS18.

With the formation of the $[(Cr-Se)/Se]_n$ multilayer the free energy of the system is assumed to be in a local minimum. Further heating leads to a reaction of the metastable intermediate, and the tetrahedral coordination of Se in the Cr−Se layers changes as can be seen from the absence of a preedge peak in the XANES of the completely interdiffused alloy (Figure 2j). After the XAS experiment isothermal annealing of the sample CS18 was continued at 240 °C. The multilayer reflection in the XRR curve vanishes, indicating that the compositional modulation completely breaks down during the next reaction step (Figure 5). The interdiffusion of a modulated structure at a given temperature obeys the equation[39]

$$\frac{d}{dt}[\ln A] = -\frac{8\pi^2}{\Lambda^2}\tilde{D}_\Lambda \qquad (2)$$

where A denotes the amplitude of the composition modulation, A^2 is directly related to the intensity of the superstructure reflection I/I_0, Λ is the wavelength of the modulation wave, and $\tilde{D}_\Lambda$ is the effective interdiffusion coefficient, and depending on Λ, it can be measured with the modulated structure technique down to 10^{-27} m^2 s^{-1}.[33] $\tilde{D}_\Lambda$ was determined for CS18 from the terminal gradient of the intensity plot (Figure 4) according to eq 2. The effective interdiffusivity for the diffusion process from the intermediate $[(Cr-Se)/Se]_{10}$ multilayer ($\Lambda \approx 60$ Å) to the nonmodulated Cr/Se alloy at 240 °C is 8.27×10^{-23} m^2 s^{-1}. This is in the range previously reported for amorphous multilayers.[37,38]

Above 250 °C a homogeneous amorphous Cr−Se alloy exists. Superstructure reflections have disappeared, and no other reflections except that of the substrate are observed in the high-angle region of the XRD patterns for all samples. EDX analyses revealed that there was no significant change of the sample composition so far. It is noted that annealing was done under dynamical vacuum conditions and consequently Se might be evaporated from the sample and is pumped away by the vacuum system. The existence of the amorphous alloy covers a wide temperature range from approximately 300 to 500 °C.

A reaction interrupted at 300 °C yields a sample of the amorphous Cr−Se alloy with 46(5) at. % Cr (sample CS13, Table 1). Within the limits of accuracy this composition is very near to the Cr:Se ratio in Cr_3Se_4 and can thus be assumed to be representative for the structural situation in the amorphous alloy directly before the nucleation of Cr_3Se_4. The XANES of the amorphous sample CS13 and of the crystalline sample CS08 evidences that the environment of Se is quite similar in both samples, because only minor differences can be seen in the two spectra (Figure 2j,m). In the amorphous alloy, the degree of order is still low and only one coordination shell can be detected in the FT-EXAFS (Figure 2l). Se−Cr distances have shortened to 2.51(1) Å, which might again be a result of the compaction of the material. The Cr−Se bond lengths are still in the typical range reported for chromium selenides in the literature. Further annealing leads to crystallization of Cr_3Se_4, and in the FT-EXAFS of a sample obtained at 660 °C three ordered shells around the Se atoms are now distinguishable (sample CS08, Figure 2o). Sample CS08 has lost approximately one-third of its initial Se content due to evaporation of Se at temperatures above 300 °C. The composition after annealing

(39) Greer, A. L.; Saepen, F. In *Synthetic Moldulated Structures*; Chang, L., Giessen, B. C., Eds.; Academic Press: New York, 1985; pp 419−486.

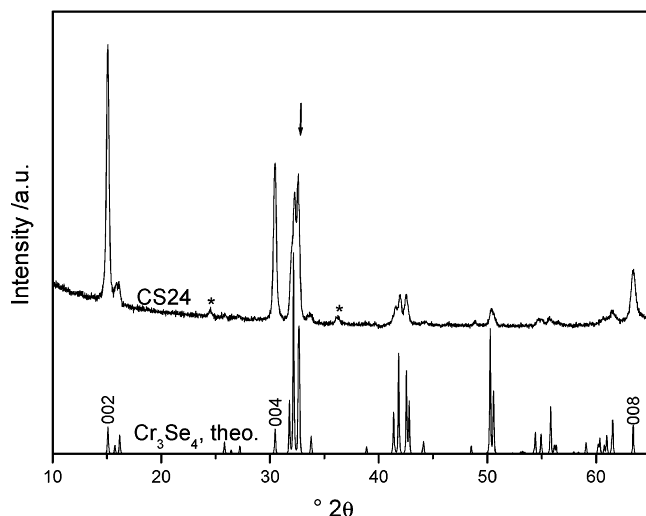

Figure 6. X-ray diffraction pattern of the sample CS24 and the theoretical powder pattern of Cr_3Se_4 calculated from single-crystal data. The pattern is dominated by the 00*l* reflections due to a pronounced texture of the thin film sample. Data for CS24 was shifted by an arbitrary amount on the intensity axis. At 33.0° 2θ (position of the arrow) the $\lambda/2$ reflection of the 400 Si substrate peak overlaps with the reflections of Cr_3Se_4. Peaks marked with an asterisk cannot be identified.

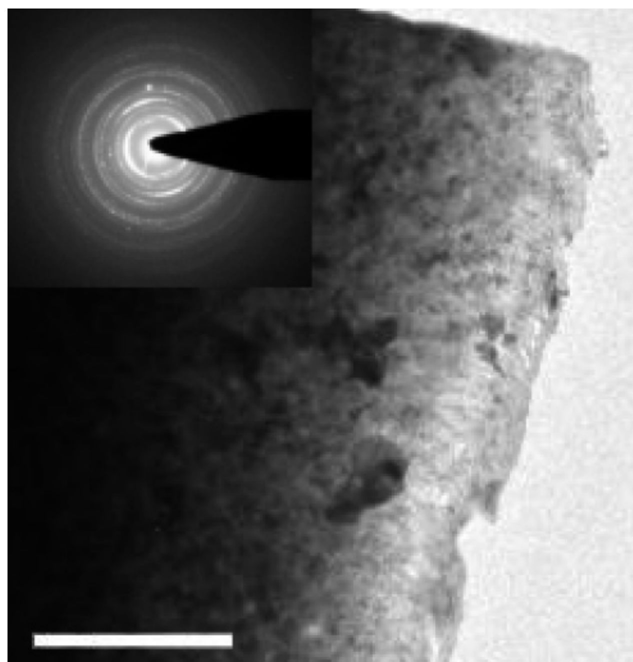

Figure 7. TEM micrograph of the free-standing Cr_3Se_4 film of sample CS21, plane view, and corresponding electron diffraction pattern (upper left corner). The white bar measures 2 μm.

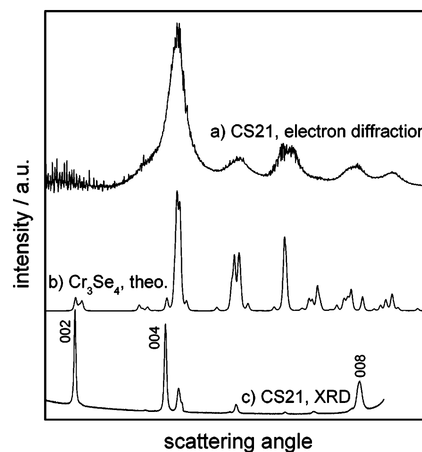

Figure 8. Integrated intensity of the electron diffraction rings in Figure 7 (a). Theoretical X-ray diffraction pattern of Cr_3Se_4 (b). Experimental XRD pattern of the sample CS21 in reflection geometry (c). Patterns were shifted by an arbitrary amount on the intensity axis.

was $Cr_{2.9(6)}Se_4$. XRD revealed that no phases other than Cr_3Se_4 were present in CS08. Concerning the first coordination shell, it can be concluded from the EXAFS that the local environment around Se in the amorphous alloy already resembles the crystalline state.

From these results the process of crystallization may be described as the setup of long-range order between existing building units without major movements of the atoms. The appearance of reflections in the high-angle region of the in situ XRD patterns indicates the start of crystallization at approximately 500 °C. The reflections in powder pattern can be indexed as highly textured Cr_3Se_4. The crystallographic *c*-axis is orientated perpendicularly to the substrate surface, and the XRD patterns are dominated by the (00*l*) series (Figure 6).

An electron diffraction study was performed on the film CS21, which was previously annealed to 650 °C. A TEM micrograph and the corresponding electron diffraction pattern are shown in Figure 7. Texture causes a strong nonuniformity of the diffraction rings. Single diffraction spots are due to residuals of the Si wafer. A full integration of the intensities of the rings gives the pattern shown in Figure 8a. Despite the poorer angular resolution of the electron diffraction data, the resulting diffraction pattern is in good agreement with theoretical X-ray data for randomly orientated Cr_3Se_4 (Figure 8b,c). It is noted that integrated peak intensities in X-ray and electron diffraction patterns cannot be compared directly.

Using the (00*l*) reflections (Figure 8c) a value for the *c*-axis of 11.82(1) Å is calculated which is about 0.1 Å larger than expected for stoichiometric Cr_3Se_4. The slight elongation is understood on the basis of the results of Maurer and Collin, who investigated the structural properties of $Cr_{3\pm x}Se_4$ ($0 < x < 0.2$) as a function of x.[20] According to their results Cr rich samples have larger unit cell parameters than Cr poor samples due to the filling of void sites in the lattice. The EDX analysis performed on the free-standing film in the TEM yields as composition $Cr_{3.3(1)}Se_4$ in the sample CS21 after annealing. The larger value for the *c*-axis is in good agreement with the surplus of Cr.

The simultaneous growth of the reflections is accompanied by a decrease of the widths of the reflections. Integral breadths of the (002), (004), and (008) peaks of CS08 were determined for various sample temperatures and corrected for instrumental line broadening. A Williamson−Hall plot was used to determine the nature of the reflection broadening.[40] The reciprocal integral breadths $\beta_f{}^*$ are plotted versus reciprocal *d* spacing d^*, clearly showing the absence of a positive slope (Figure 9a). The line profile is independent of the diffraction angle; i.e., line broadening is caused by

(40) Williamson, G. K.; Hall, W. H. *Acta Metall.* **1953**, *1*, 22−31.

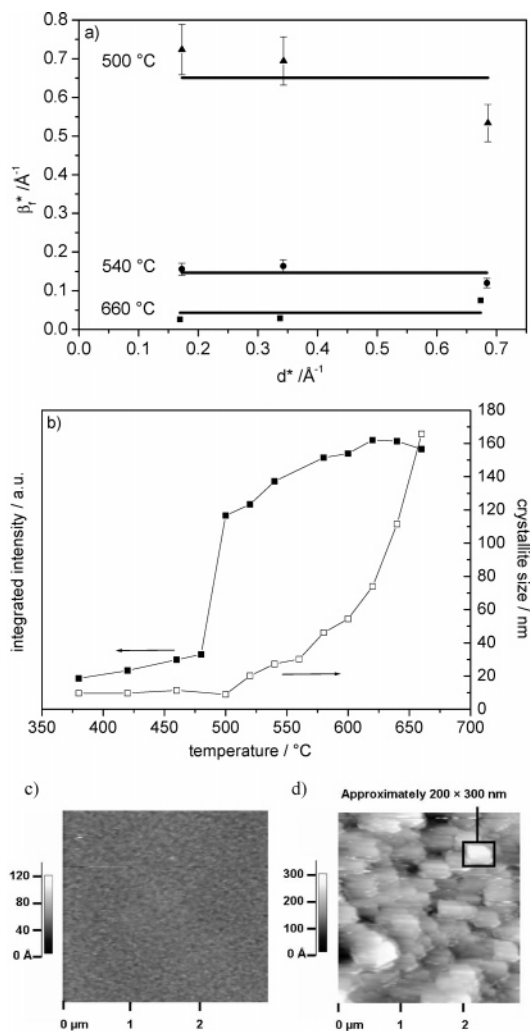

Figure 9. Williamson–Hall plot for the profiles of the 002, 004, and 008 reflections of Cr_3Se_4 (CS08) at different temperatures. The lines represent horizontal fits to the data and serve as guide for the eyes. Errors were determined on the basis of the *R*-parameters of the fit, and error bars are shown where they exceed the symbol size. (a). Integrated intensity of the (00*l*) reflections and apparent crystallite sizes as functions of annealing temperature. The lines are drawn as guides for the eye (b). AFM pictures of the sample CS08 as deposited (c) and after annealing (d).

crystallite size effects, and strain can be neglected as expected at temperatures around 500 °C. The apparent crystallite sizes were determined using the Scherrer equation and are plotted together with intensity data in Figure 9b. Crystallization of the material starts at 480 °C quite abruptly from nuclei with size between 100 and 200 Å in the *c*-axis direction, which is about 10–20 unit cells. The abrupt increase of reflection intensity is accompanied by very little increase of the crystallite size. An explanation for these findings is that nuclei are formed simultaneously at many different sites in the film at this temperature and the amorphous alloy is consumed. The crystallite size and the integrated intensity curves develop in the same manner in the temperature range of 520–580 °C, indicating that the nuclei grow on the cost of the amorphous material. Pronounced crystallite growth starts at higher temperatures around 550 °C. The total amount of diffracted intensity is saturated at this temperature, indicating that the whole film has crystallized and the bigger crystals grow at the cost of the smaller ones from now on. This process is not finished at 660 °C, which was the upper temperature limit of the experiments. The crystals exhibit an apparent average size of 160 nm after the heat treatment. The sample CS08 is roughly 200 nm thick so that in average only one grain boundary is present over the full film thickness. The surface topology of sample CS08 was investigated with AFM. Upon annealing, the root mean square (rms) surface roughness has increased from 5 to 40 Å due to the formation of crystallites at the surface. Their sizes in the lateral dimensions were estimated to approximately 200 × 300 nm (Figure 9c), which is close to results determined with LPA of XRD data for the direction perpendicular to the substrate surface. However, both methods are not entirely comparable because LPA yields apparent sizes only, which usually are smaller than the average real crystal sizes,[27] and the surface crystallites monitored with AFM are not necessarily representative for inner grains. On the other hand, platelike crystal morphology is often found for chromium selenides. One should keep in mind that only the average size can be determined with LPA (line profile analysis), but no information is obtained about the distribution of crystallite sizes.

Cr_3Se_4 was produced after the amorphization in all our samples around 500 °C. Surprisingly, the initial composition of the as deposited films has only a minor influence on the reaction pathway. It was shown by Johnson and co-workers for reactions of elemental modulated reactants in other systems that the reaction mechanism and also the products obtained can depend strongly on the composition of the amorphous intermediate.[41] Those samples typically have a constant composition during the reaction. The samples of this study were annealed in a nonclosed system, and Se was evaporated at temperatures between 300 and 500 °C. Consequently, all initially Se-rich samples exhibit a composition near Cr_3Se_4 after annealing. Samples with an initial large excess of Se were found to give much stronger and sharper reflections of Cr_3Se_4 in the XRD patterns than the initially Se-poor samples. The surplus of Cr present in samples with a composition of Cr:Se > 3:4 could not be detected by XRD, indicating that Cr_3Se_4 grains exist in a matrix of amorphous Cr. It can be assumed that Cr_3Se_4 crystallizes until Se is exhausted, leaving the excess Cr in the amorphous state. These samples are thus not single-phased, and the XAS results obtained from phase-pure samples can be assumed to be only representative for the structural situation in the Cr_3Se_4 grains. It is noted that films of amorphous Cr can be produced by full evaporation of Te from Cr/Te films.[11] Cr does not crystallize at temperatures as high as 750 °C in such thin film samples. The loss of Se in the initially Se-rich samples was up to one-third of the initial Se content, and a composition near Cr:Se = 3:4 was reached after annealing. Initially Cr-rich samples lost around 10–15% Se. For example, the samples CS03, CS10, and CS11 exhibit 25(5), 29(5), and 26(5) at. % Se, respectively, after annealing to 600 °C.

(41) Johnson, C. D.; Anderson, K.; Gromko, A. D.; Johnson, D. C. *J. Am. Chem. Soc.* **1998**, *120*, 5526–5232.

When Se is evaporated during the heating process from the samples with an initial Se content above 60 at. %, these films will temporary reach the stoichiometry Cr_2Se_3 (60 at. % Se) prior to Cr_3Se_4 (57 at. % Se). Cr_2Se_3 is a stable phase in the Cr−Se phase diagram but was not found to crystallize from any of our samples. The suppression of crystallization of Cr_2Se_3 from initially Se-rich samples might be related to a high nucleation barrier. In the syntheses from modulated thin film reactants the nucleation barriers play a key role in what phases crystallize. Hence, despite the correct composition of a distinct phase such as Cr_2Se_3 in the present study a different compound crystallizes due to the significantly lower nucleation barrier. The observation made for the Cr−Se system is not unique, and a similar finding was reported for the Ni−Ge system.[42]

Since amorphization was observed for all samples in this study, no "critical thickness" could be found for Cr/Se multilayer samples with a double-layer thickness of up to 200 Å.

Conclusion

The reaction of Cr/Se multilayers was investigated using various techniques. The existence of an interdiffusion intermediate was established for Cr-rich multilayers (CS05, CS18) that give XRR data of a better quality than Se-rich samples. The formation of the intermediate was related to the Cr/Se single layer thickness ratio in the repeating double layer, which is less than 1. In Se-richer samples this ratio should favor the formation of the intermediate even more, so the intermediate can be assumed to be a general feature in the reaction of the samples.

Under this assumption, a general mechanism of the reaction can be proposed which is schematically shown in Figure 10. Artificially modulated structures exhibit a large amount of free energy. It was shown that the relaxation of the Cr/Se multilayers (Figure 10a) into states of lower energy occurs stepwise via two intermediates. In a first step, the single layers interdiffuse and form an intermediate $[(Cr-Se)/Se]_n$ multilayer at about 200 °C (Figure 10b). Se atoms reside in a tetrahedral coordination environment in the Cr−Se layers. Further annealing leads to complete destruction of the compositional modulation. The effective interdiffusion coefficient for this reaction step was determined. The pronounced densification of the samples that can be seen from the shift of the multilayer XRR peak is also probed by the shrinking distances for both Se−Se and Se−Cr contacts during annealing. A homogeneous amorphous Cr−Se alloy is formed and stable up to approximately 500 °C (Figure 10c). Se is lost from the alloy at this stage by evaporation resulting in a composition near 57 at. % Se

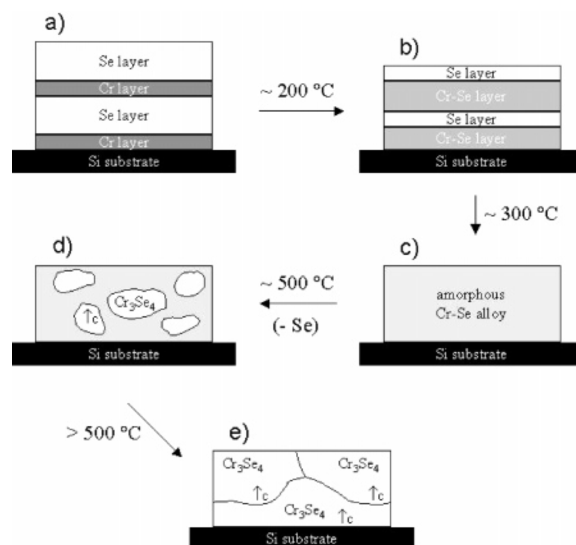

Figure 10. Schematic representation of the three-step reaction of Cr/Se multilayers under the selected conditions (see text). The $[Cr/Se]_n$ multilayer (a, only two double layers are shown) interdiffuses in a first step to form an intermediate $[(Cr-Se)/Se]_n$ multilayer (b). The interdiffusion continues, and an amorphous Cr−Se alloy is formed (c). Textured Cr_3Se_4 crystallites from nuclei of approximately 10−20 Å around 500 °C (d) (crystallite sizes are not scaled to the initial layers thickness). The Cr_3Se_4 crystals grow until only a very few grain boundaries can be found over the full film thickness (e).

for the initially Se-richer samples. The local structure around the Se atoms prior to crystallization already resembles the environment in the crystalline product Cr_3Se_4. Nucleation occurs abruptly at ca. 500 °C and can be regarded as the setup of long-range order with no major changes in the connectivity of the atoms (Figure 10d). Subsequent crystallite growth leads to grain sizes comparable with the total film thickness for initially Se-rich samples (Figure 10e), whereas the initially Se-poor samples are assumed to stop at the stage depicted in Figure 10d, exhibiting Cr_3Se_4 grains in a matrix of amorphous Cr.

The modulated elemental reactant method was shown to be an effective way to synthesize thin films of amorphous and crystalline Cr_3Se_4 and to shed light on their solid-state reaction mechanism.

Acknowledgment. We thank HASYLAB for the allocation of beam time, Dr. Julia Wienold of HASYLAB for the support with the XAS measurements, and Dipl.-Chem. Henning Lühmann for the preparation of the reference Cr_3Se_4 sample. We gratefully acknowledge the financial support of the state of Schleswig-Holstein, the Fonds der Chemischen Industrie (FCI), the Bundesministerium für Bildung und Forschung (BMBF), and the Deutsche Forschungsgemeinschaft (DFG).

IC0515204

(42) Jensen, J. M.; Ly, S.; Johnson, D. C. *Chem. Mater.* **2003**, *15*, 4200−4204.